Chem

CellPress

Article

Controllable Growth of (n, n −1) Family of Semiconducting Carbon Nanotubes

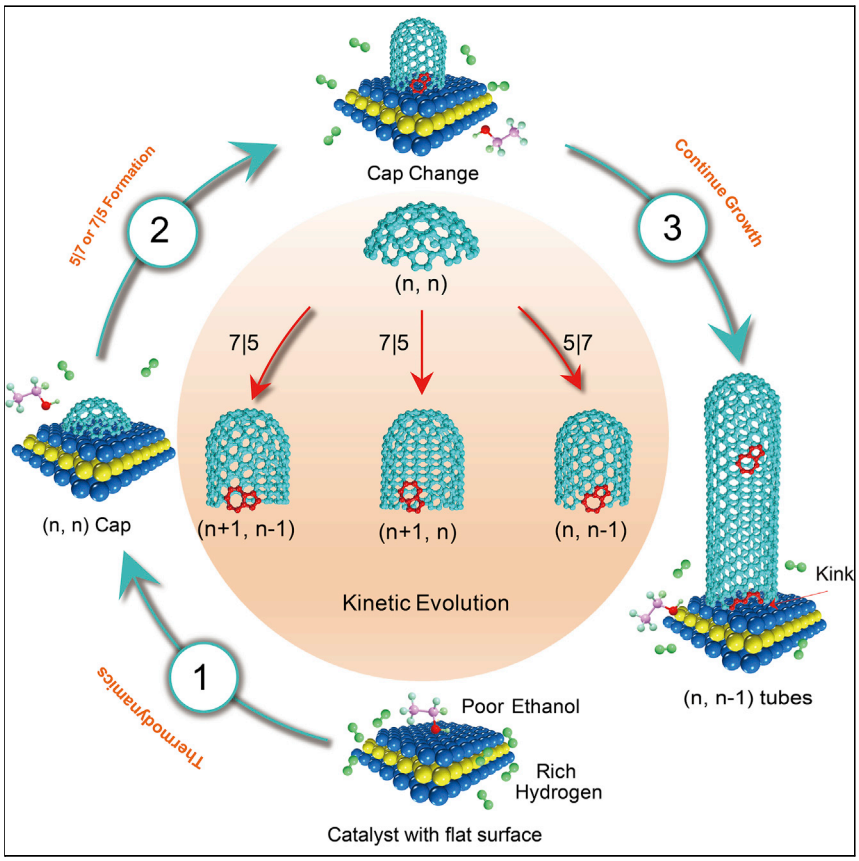

Zhang and co-workers developed a rational approach to growing a new family of semiconducting SWNTs: (n, n − 1) carbon nanotubes. Combined with catalyst design, both large-diameter (>2 nm) (n, n − 1) SWNTs and single-chirality (10, 9) SWNTs with abundances of 88% and >80%, respectively, were successfully realized. This strategy opens up a new route for the growth of SWNT families beyond catalyst design.

Shuchen Zhang, Xiao Wang, Fengrui Yao, ..., Kaihui Liu, Feng Ding, Jin Zhang

f.ding@unist.ac.kr (F.D.)
jinzhang@pku.edu.cn (J.Z.)

HIGHLIGHTS

Near-equilibrium growth process

A kinetics mutation mechanism

Large-diameter (n, n − 1) carbon nanotubes with abundance of 88%

Single-chirality (10, 9) carbon nanotubes with abundance of 80%

Zhang et al., Chem 5, 1182–1193
May 9, 2019
https://doi.org/10.1016/j.chempr.2019.02.012

Chem

CellPress

Article

Controllable Growth of (n, n −1) Family of Semiconducting Carbon Nanotubes

Shuchen Zhang,[1,7] Xiao Wang,[2,7] Fengrui Yao,[3] Maoshuai He,[4,5] Dewu Lin,[1] He Ma,[3] Yangyong Sun,[1] Qiuchen Zhao,[1] Kaihui Liu,[3] Feng Ding,[6,*] and Jin Zhang[1,8,*]

SUMMARY

Semiconducting single-walled carbon nanotubes (SWNTs) with controlled chirality (n, m) and band gaps are expected to create a new era of electronics. Here, we report a rational design to enable SWNTs' near-equilibrium nucleation and then grow a new family of semiconducting SWNTs: (n, n − 1) carbon nanotubes. No metallic SWNTs were observed in ~100 samples by reflection optical spectral measurements. Combined with catalyst controlling, we have successfully synthesized both large-diameter (>2 nm) (n, n − 1) SWNTs and single-chirality (10, 9) SWNTs with abundances of 88% and >80%, respectively. Theoretical analysis indicates that the chirality of (n, n) tubes tends to change to (n, n − 1) by kinetically incorporating an energetically preferred pentagon-heptagon pair in the tube wall. This strategy opens up a new route for the growth of SWNT families beyond catalyst design.

INTRODUCTION

Semiconducting single-walled carbon nanotubes (SWNTs) with controlled band gaps are thought to create a new era of electronics.[1–4] To realize this goal, major efforts have been devoted to obtaining SWNTs with uniform properties or structure,[5–9] such as by solution separation,[5] by controlled chemical vapor deposition (CVD)[6] and even by growing SWNTs with specific helicity (n, m) controlled by a catalyst.[7–9] Especially, strategies for directly synthesizing semiconducting SWNTs beyond catalyst design are highly desirable. On the basis of their electronic properties and structures, the helicities of SWNTs can be divided into different families, (n, n − i), where SWNTs belonging to the family of mod(i, 3)=0 are conducting and are otherwise semiconducting.[10] Currently, semiconducting SWNTs used in electronic applications are mainly obtained by solution separation,[5] although CVD growth,[11,12] if possible, is highly preferred because of the long pristine SWNTs obtained without pollution. Selective growth of s-SWNTs has been realized via catalyst control,[13,14] selective etching,[15–17] and over-controlled chirality-specific dominant growth,[18–20] which is achieved only in very strict experimental conditions. These methods provide finite control but limited species. Recently, (2m, m) SWNTs as a family have been reported to be selectively enriched with tungsten carbide (WC) or Mo_2C, independently of catalyst size, but the tubes are still mixed semiconducting and conducting.[21] In principle, the direct synthesis of (n, n – 3i + 1) or (n, n – 3i + 2) families of SWNTs, such as the near-armchair (n, n − 1) or (n, n − 2), makes semiconducting SWNTs feasible. In this approach, the precise control of the catalyst particles, which is the most challenging part of all CVD experiments, is also not necessary.

Previous studies[22–24] and our calculations shown below demonstrate that epitaxial SWNT growth is templated by the catalyst, and a flat low-index catalyst surface favors tight contact with the flat open end of a SWNT. Among all the SWNTs, only

The Bigger Picture

Semiconducting single-walled carbon nanotubes (SWNTs) with controlled chirality (n, m) and band gaps are expected to create a new era of electronics. Recent progress has enabled the synthesis of (2n, n) SWNTs by designing unconventional solid catalysts, which is very challenging experimentally. Strategies for synthesizing semiconducting SWNTs beyond catalyst design are highly desirable. Herein, we report a rational design to enable SWNTs' near-equilibrium nucleation and then grow a new family of (n, n − 1) semiconducting SWNTs, including large-diameter (>2 nm) (n, n − 1) SWNTs and single-chirality (10, 9) SWNTs with abundances of 88% and >80%, respectively. This strategy opens up a new route for the growth of SWNT families beyond catalyst design.

the achiral armchair (n, n) and zigzag (n, 0) tubes own flat open ends, but their growth rates are extremely low because of the lack of active sites (kinks) at the SWNT-catalyst interface.[24–26] As demonstrated in Figure 1, a highly stable (n, n) tube cap on a flat catalyst surface may grow into a short (n, n) SWNT via a repeatable ring-by-ring growth. As a consequence of achiral structure, (n, n) tubes would overcome a significant energy barrier (e.g., ~2.36 eV for (9, 9) tubes) in the growth of each carbon ring, whereas a structure mutation is introduced to produce a kink that leads to the continued growth without a barrier. At the same time, the structure mutation also brings a change in chirality[27,28] from the slow-growing (n, n) SWNT to a fast-growing chiral SWNT. For such "structure mutation," the addition of an adjacent pentagon-heptagon pair (5|7) is known as the energetically most preferable route for tube mutation, and such a 5|7 in a tube wall may turn the helicity of the SWNT to (n, n − 1), (n + 1, n), and (n + 1, n − 1) SWNTs depending on the orientation of the 5|7 pair. So, in principle, if the (n, n) caps or short tubes can be stabilized during the nucleation stage, the selective growth of (n, n − 1) and (n, n − 2) families of SWNTs is possible. Applying similar analyses, as shown in Scheme S1, the growth of (n, 1) SWNTs is possible if the achiral (n, 0) caps or short SWNTs can be stabilized.

RESULTS AND DISCUSSION

According to Figure 1, the (n, n − 1) tubes could be widely realized on many different catalysts, including traditional catalysts, such as Fe, Co, and Ni. Considering the proper activity and specific structure, Co catalysts were chosen in our experiment, and the near-equilibrium growth condition was explored by tuning the C/H ratios. The theory of crystal growth states that the preferential growth of the highly stable nuclei requires a long incubation time or near-equilibrium growth, and it is necessary to minimize the tube growth rate, which is related to the tube length. The tube length as a function of time observed with four different carbon-supply-to-hydrogen ratios (C/H = 50/400, 40/400, 25/400, and 15/400) is shown in Figure 2A. Although precise measurement of the incubation time is very difficult, the significant reduction of the growth rate is clearly seen. As expected, the chiral-angle distributions measured by chirality analysis in reflection optical spectra (Figure 2B) indicate an obvious tendency to the preferential growth of large chiral-angle SWNTs when the C/H ratio is low, although the tubes are short (Figure S4). Electron diffraction patterns (EDPs) were also performed to prove the chirality (shown in Figure S11). Further, a broad catalyst-size distribution is shown in Figure 2C (obtained from Figure S3), proving that these tubes obtained by Co catalysts with large chiral angles were free of catalyst size distribution. Further reflection optical spectrum analysis showed that the total population of the (n, n − 1) family of SWNTs, including (13, 12), (15, 14), (16, 15), and (18, 17), is ~ 88%, and these tubes have nearly 3-fold symmetry (Figure 2D). It is worth noting that the total population of (n, n − 1) and (n, n − 2) SWNTs reaches ~97%, and all the identified SWNTs are semiconducting, which is very different from that of tubes obtained by large C/H ratios (shown in Figures S6 and S7).

As shown in Figure 2E, transmission electron microscopy (TEM) shows that the (1 1 1) surface of a Co catalyst particle provides the template for SWNT growth. Obviously, the size of the catalyst is larger than the diameter of the corresponding tube, which shows that it conforms to the perpendicular model. To further prove the stable structure of Co catalysts at 850°C, high-resolution TEM (HRTEM) was applied to observe the state of the catalysts *in situ* heating with 200 kV, and the results with different times are shown in Figure 2F. Three catalysts with different sizes (3.314, 2.543, and 2.701 nm) were observed, which indicates that the catalysts still maintained the solid-state and stable structures after 10 min of heating.

[1]Center for Nanochemistry, Beijing Science and Engineering Center for Nanocarbons, Beijing National Laboratory for Molecular Sciences, Key Laboratory for the Physics and Chemistry of Nanodevices, College of Chemistry and Molecular Engineering, Peking University, Beijing 100871, China

[2]Center for Multidimensional Carbon Materials, Institute for Basic Science, Ulsan 44919, South Korea

[3]State Key Laboratory for Mesoscopic Physics, School of Physics, Collaborative Innovation Center of Quantum Matter, Peking University, Beijing 100871, China

[4]Key Laboratory of Eco-Chemical Engineering, Ministry of Education, College of Chemistry and Molecular Engineering, Qingdao University of Science and Technology, Qingdao 266042, China

[5]School of Materials Science and Engineering, Shandong University of Science and Technology, Qingdao 266590, China

[6]School of Materials Science and Engineering, Ulsan National Institute of Science and Technology, Ulsan 44919, South Korea

[7]These authors contributed equally

[8]Lead Contact

*Correspondence: f.ding@unist.ac.kr (F.D.), jinzhang@pku.edu.cn (J.Z.)

https://doi.org/10.1016/j.chempr.2019.02.012

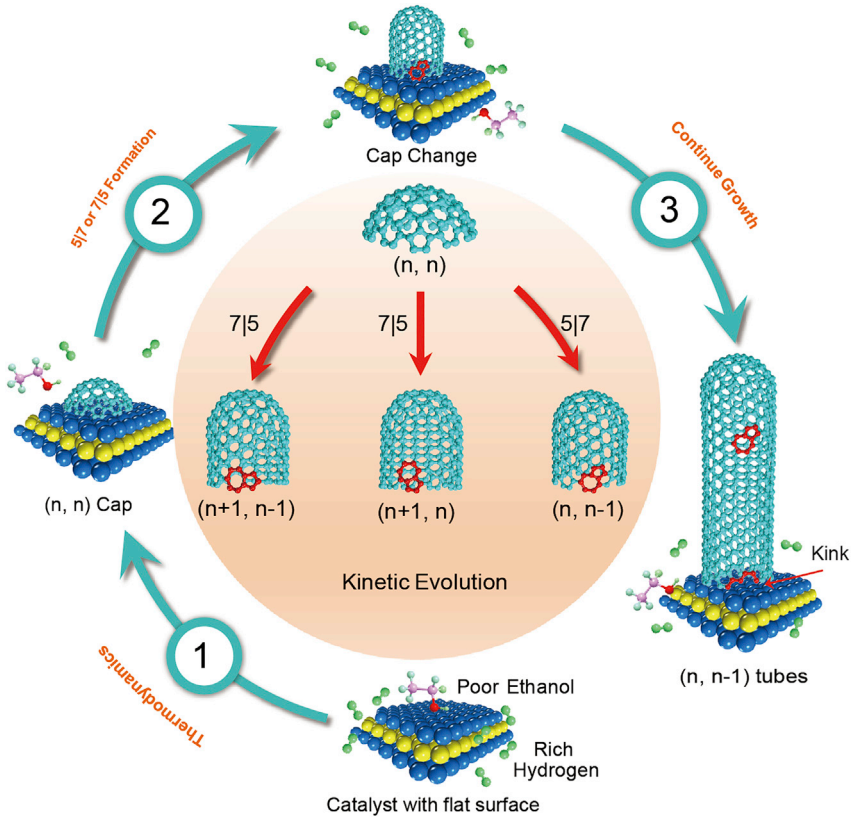

Figure 1. Schematic Illustration of the Mechanism of Selective (n, n − 1) and (n, n − 2) SWNT Growth

If a high hydrogen-carbon ratio is used to realize the near-equilibrium growth of carbon nanotubes in this growth condition, it will happen as follows: (1) a highly stable armchair SWNT cap will form on a flat catalyst surface, (2) a possible SWNT mutation will change the (n, n) SWNT into a (n, n − 1) or (n, n − 2) SWNT, and (3) the (n, n − 1) will grow quickly with an active site (kink).

Then, to understand the growth mechanism of (n, n − 1) tubes, we performed theoretical calculations, as shown in Figure 3. Considering the different relative stabilities of different SWNTs on the Co (1 1 1) surface, the formation energies of serial SWNTs with similar diameters to the (9, 9) SWNT were calculated (Figures S13 and S14). As shown in Figure 3A, the (9, 9), SWNT had the lowest formation energy (optimized structure shown in Figure S15), and the (15, 0) SWNT was found at a local minimum in the energy profile. This result supports the assumption that armchair caps or shorter SWNTs can be preferentially nucleated under the condition of near equilibrium. In addition, the formation energies of near armchair tubes, such as (9, 8), (10, 9), and (10, 8), are lower than most SWNTs except the armchair ones, indicating the energetic advantage of the (n, n − 1) and (n, n − 2) SWNTs. These analyses imply that the growth of a SWNT with a low carbon supply may start with an armchair cap or a short armchair SWNT. We used the (9, 9) tube as an example to demonstrate the evolution of the armchair SWNT during further growth. As shown in Figure 3B, we obtained the (9, 9) SWNT by adding carbon atoms ring by ring with an energy barrier of ~ 2.36 eV, indicating that the growth rate of the (9, 9) SWNT must be extremely slow. To accelerate the growth of the (9, 9) SWNT, we considered the addition of a 5|7 ring pair into the SWNT wall during growth. Depending on the orientation of the 5|7, the chiral SWNT might be (9, 8), (10, 9), or (10, 8), each of which has active kink sites at the edge for carbon insertion and therefore can grow orders of

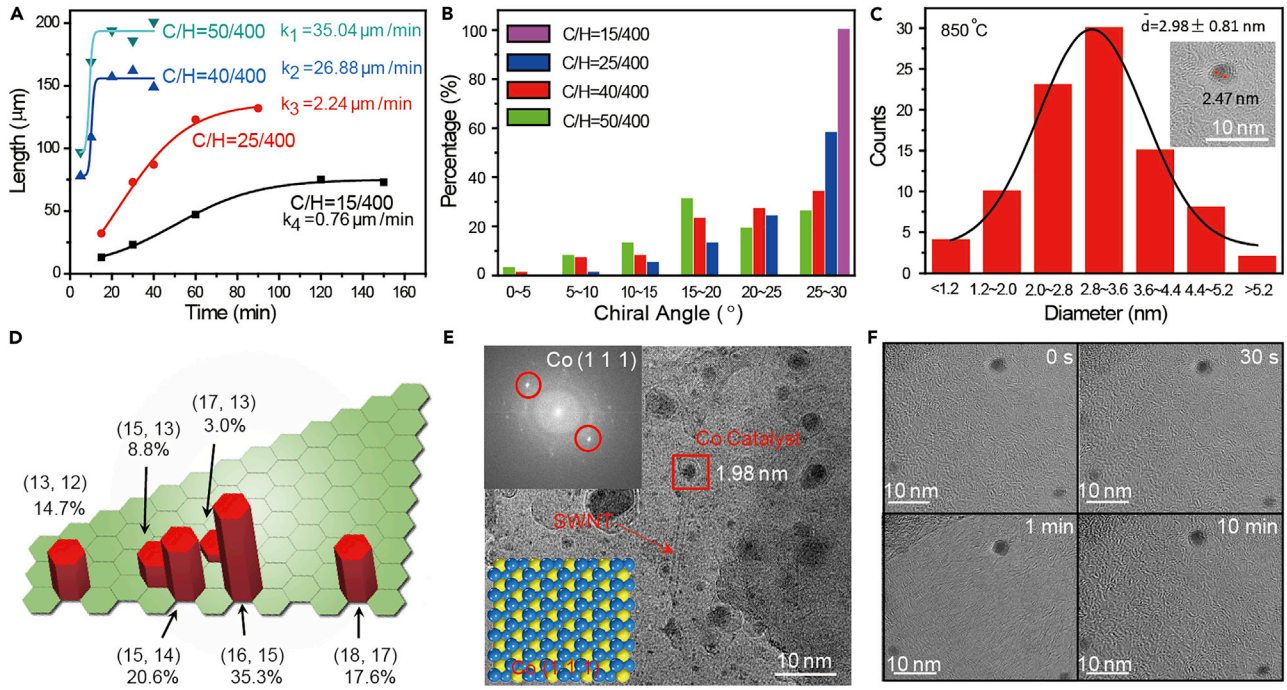

Figure 2. Realization of (n, n − 1) Tubes Near-Equilibrium Growth and Solid Co Catalysts as a Growth Template

(A) Length distribution with different growth time and C/H ratios for evaluating the growth rate. The C/H ratio is defined by the specific flow of ethanol and hydrogen.

(B) The chiral angle distributions of SWNTs obtained with different C/H ratios were calculated from the reflection optical spectra. With the C/H ratio of 15/400, the tubes are mainly near-armchair tubes with large chiral angles and narrow distributions.

(C) The size distribution of Co catalysts obtained at 850°C, where the mean diameter is 2.98 nm.

(D) The specific-chirality distribution of tubes obtained with the C/H ratio 15/400 from reflection optical spectra shows that the tubes are mainly (n, n − 1) tubes.

(E) TEM image indicates that an individual SWNT was grown from the Co (1 1 1) plane. The insets are the FFT of Co catalyst and the Co (1 1 1) atomic model.

(F) Observation of *in situ* heating at 850°C by HRTEM at different times: 0 s, 30 s, 1 min, and 10 min. The catalysts have a better thermal stability and keep solid state at a high temperature.

magnitude faster than the (9, 9) SWNT (shown in Figures S16–S18). The estimated transition barriers are 3.8, 4.87, and 5.8 eV for (9, 8), (10, 9), and (10, 8) SWNTs, respectively, as shown in Figure S19 and Table S4. This implies that growth of the (n, n − 2) family of SWNT is more difficult than that of the (n, n − 1) family of SWNTs, which agrees very well with the experimental observations that (n, n − 2) tubes had only about 9% abundance.

To explore further details of (n, n − 1) SWNT growth, we considered the symmetry of the SWNT-catalyst interface. The Co (1 1 1) surface has a 3-fold symmetry and therefore has atomic matching to a 3-fold armchair SWNT, such as (6, 6), (9, 9), (12, 12), or (15, 15), and this catalyst surface should be more energetically preferred. As an example, Figure 3C shows the high stability of the (9, 9) SWNT on the Co (1 1 1) surface in comparison with others. This analysis further predicts the preferential growth of the (3n, 3n) caps or short (3n, 3n) SWNTs during the nucleation stage of the SWNTs. With the mutation mechanism discussed above, we can predict that the most preferred (n, n − 1) SWNTs are (9, 8), (10, 9), (12, 11), (13, 12), (15, 14), (16, 15), (18, 17), (19, 18), etc. It is interesting that because of the 3-fold symmetry of the catalyst surface, some (n, n − 1) SWNTs, such as (11,10), (14, 13), and (17, 16), do not appear in the list. By carefully comparing the experimental results

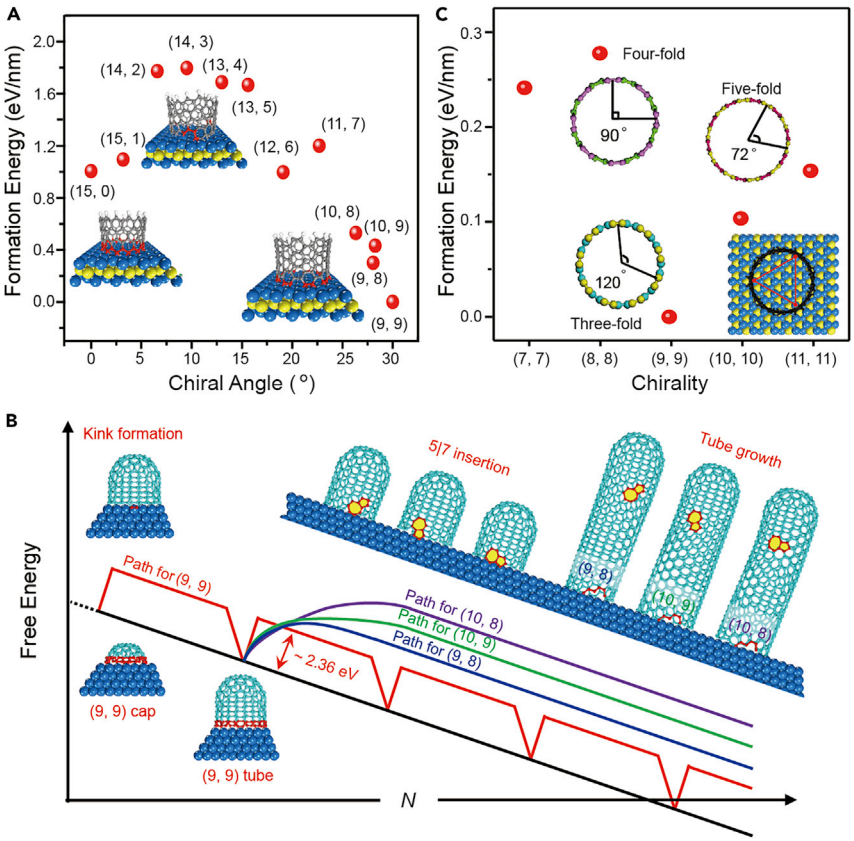

Figure 3. Theoretical Calculation Results and Scheme to Understand the Growth Mechanism of (n, n − 1) Tubes

(A) The formation energies of different tubes on a Co (1 1 1) flat surface.

(B) The high barrier in each cycle of growth for a (9, 9) tube leads to a mutation of chirality by introducing a 5|7 defect.

(C) Symmetry matching between tubes and Co (1 1 1) face leads to the lowest formation energy of the (9, 9) tube.

shown in Figure 2D, we confirmed the absence of the (14, 13) and (17, 16) SWNTs. The agreement between the theoretical prediction and the experimental observation validates the mutation mechanism for the growth of the (n, n − 1) SWNTs and (n, n − 2) SWNTs. Moreover, ferromagnetic metals showed better selectivity than other catalysts. For Cu catalysts, it is much harder to form solid catalysts in that they have a lower melting point, but for Mo, the main reason is the high catalytic activity when it transforms into Mo_2C to lead to the formation of other SWNTs, as proved in Figure S8 and Tables S1–S3.

It is worth noting that the amounts of hydrogen in the system will weaken the catalysts activity seriously and bring a low density of (n, n − 1) tubes. To improve the density, we designed a stack-up substrate, as shown in Figure S1, with quartz and Si/SiO_2 (300 nm) and introduced CO_2 as the etchant to keep the near-equilibrium growth condition. In Figures 4A and S2, the gap is about 20 μm, and the gas is mainly diffused into the gap. The residence time of the gas in the gap was estimated to be ~0.49 s, which is longer than the substrate directly exposed to the gas. The SEM image in Figure 4B shows a higher density of tubes after introducing CO_2 as etchants and free of hydrogen. However, the tubes are randomly distributed because CO_2 would partly react with quartz substrate. As shown in Figure 4C, Raman mapping for these tubes showed that many of the

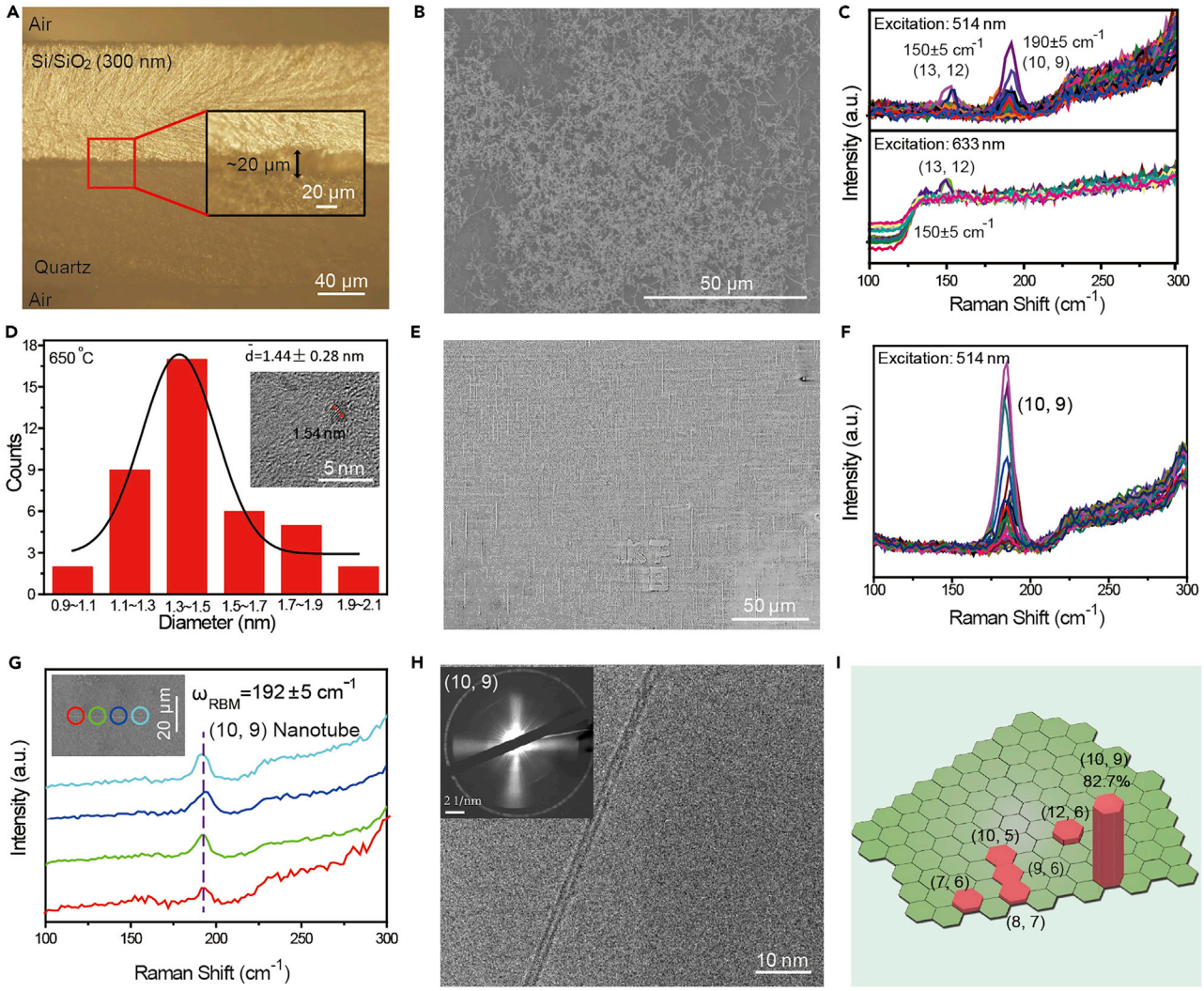

Figure 4. Stack-Up Substrate Design with CO_2 to Improve the (n, n − 1) Tube Density and Enriched Growth of (10, 9) Tubes by Controlling the Catalyst Size

(A) The gap between quartz and Si/SiO_2 (300 nm) is about 20 μm as proved by a typical optical image of the cross-section of the structure.
(B) Typical SEM image of random (n, n − 1) tubes on quartz substrate.
(C) Raman with two different lasers (514 and 633 nm) to prove that the tubes are (n, n − 1) tubes.
(D) The size distribution of Co catalysts obtained at 650°C; the mean size is 1.44 nm. The inset is a typical AFM image of the catalyst.
(E) Typical SEM image of tubes obtained with the catalysts in (D), and the tubes have the same orientation.
(F) Raman mapping with 633 nm indicates that the tubes mainly are (10, 9) according to the RBM peaks.
(G) Raman detections on different positions of the (10, 9) tube show the uniform structure.
(H) TEM image of the individual tube after it is transferred on the Cu grid; the electron diffraction pattern indicates that the tube is a (10, 9) tube.
(I) The chirality-distribution map of the as-grown tubes was found from Raman analysis. It indicates that about 82.7% of the tubes are (10, 9) tubes.

tubes are (10, 9) and (13, 12). It is important to note that the above result is achieved without careful control of the size of the Co catalyst particles. As the new strategy shrinks the SWNT's chiral map into a narrow band of (n, n − 1) SWNTs, further control of the size of the Co catalyst should allow us to synthesize only one or two specific (n, n − 1) SWNTs. To test this idea, we synthesized and characterized Co catalyst particles with a narrow diameter distribution of 1.4 ± 0.25 nm (Figure 4D). Using these catalysts, we synthesized SWNTs on quartz substrate with a C/H ratio of 10/400, and Figure 4E shows the typical SEM image. The Raman characterizations of the optimized SWNT samples are shown in Figures 4F, 4G, and S10, and to further prove the specific structure of tubes, we

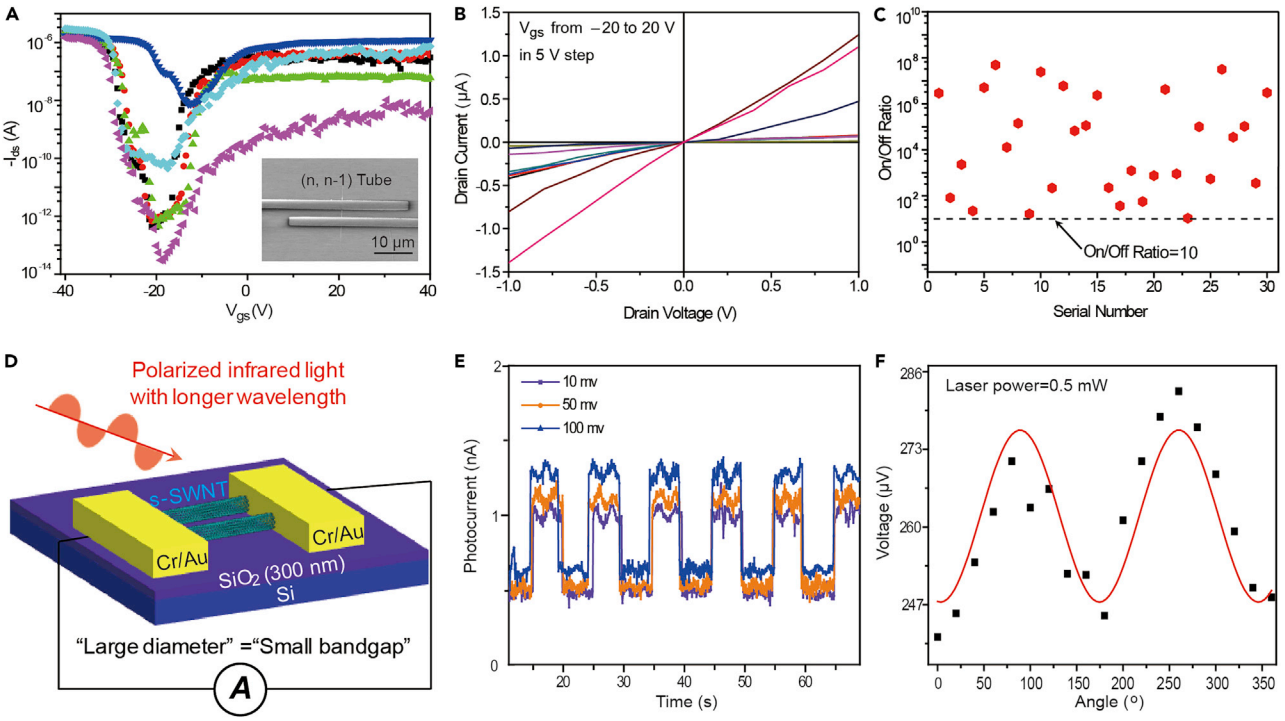

Figure 5. Electrical Performance and Broadband Infrared Photodetector of the (n, n − 1) Tube FETs

(A) Transfer characteristics of six SWNT FETs. The inset is a SEM image of an FET device fabricated with a single (n, n − 1) tube as the channel material and a channel length of 2 μm.

(B) Output (I_{ds}-V_{ds}) characteristics of one device measured at various V_{gs} from −20 to 20 V in 5 V steps.

(C) The statistical result of I_{on}/I_{off} ratios for 30 devices shows that nearly all the I_{on}/I_{off} ratios are higher than 10.

(D) Schematic diagram showing the photodetector device fabricated from aligned (n, n − 1) tubes.

(E) The evident photoresponse shown at different V_d (10, 50, and 100 mV), which is helpful for the exciton separation in the symmetry electrode. A supercontinuum laser was used as the light source, and an 850-nm long-pass filter was used to extract the infrared part of the spectrum. The sample was pumped with an incident power of 0.5 mW.

(F) Polarization-dependent photovoltage observed for the device in (D). The sample was pumped with an incident power of 0.5 mW, and a 780-nm long-pass filter was used to extract the infrared part of the spectrum.

performed EDPs based on TEM after transferring the tubes onto a copper grid, and the results are shown in Figures 4H and S12. Figure 4I shows the specific population of the (10, 9) SWNT through statistics on radial breathing mode (RBM) peaks, and it was found to be 82.7%. The success of single-chirality SWNT synthesis implies that the new strategy of SWNT structural control is independent of the catalyst design, and when used together with catalyst design, the synthesis of various SWNT families, such as (4n, 4 n − 1)/(4n, 4n + 1) or (6n, 6n − 1)/(6n, 6n + 1), is possible with a catalyst surface with a 4- or 6-fold symmetry. As shown in Figure S5, we found (13, 12) and (15, 14) tubes with near 3-fold symmetry when we used Mo_2C catalysts and found (16, 15) and (20, 19) tubes with near 4-fold symmetry when we used WC catalysts. However, the occupation was small (about 37.8%) for the high activity of carbide catalysts, as shown in Figure S4.

To utilize the semiconducting property of the (n, n − 1) tubes, we synthesized back-gated SWNT field effect transistors (FETs) as shown in Figure 5A. The transfer characteristic curves of seven devices in Figure 5A show high on/off ratios but were not uniform for the tubes used with different diameters and bipolar behaviors for their perfect structure, which was also proved by Raman characterization in Figure S9. Figure 5B shows the typical output characteristics of the FETs, indicating that ohmic contacts exist between SWNTs and metal electrodes. Many more devices were

measured, and the corresponding on/off ratio distributions were plotted in Figure 5C. Among the 30 FETs, only one of them had an on/off ratio of ~10, which indicates the semiconducting properties of the channel SWNTs. On the other hand, because the large-diameter (n, n − 1) SWNTs have small band gaps, they can be used as room-temperature broadband infrared photodetectors.[29] The (n, n − 1) tubes have a specific orientation, and therefore the photodetector fabricated by these tubes are polarization dependent. The photodetector was fabricated as shown in Figure 5D, and Figure 5E shows the evident photoresponse by using different V_d, which is helpful for the exciton separation in the symmetry electrode. Figure 5F further proves that our photodetector exhibited a strong polarization-sensitive photo signal for the specific orientation of (n, n − 1) SWNTs.

In summary, we propose a new route to controlling the structure of SWNTs in a family and have demonstrated that selective growth of (n, n − 1) semiconducting SWNTs with different diameters and bandgaps can be achieved with a low carbon supply. Theoretical analysis suggests that the preferential (n, n − 1) SWNT growth is achieved through a near-equilibrium (n, n) SWNT nucleation and a chirality mutation and further predicts catalyst-symmetry-dependent growth behavior. The experimental results are in agreement with the mechanism hypothesized by the theoretical analysis to induce the selective growth of SWNTs. This new strategy for the controllable growth of SWNTs is independent of the previous strategy of catalyst design and opens a new avenue to realizing structure control according to the SWNT family. Further, when combined with catalyst size control, it can achieve the specific-chirality growth of SWNTs for various applications

EXPERIMENTAL PROCEDURES

Growth of (n, n − 1) SWNTs on the Quartz Substrate by Stack-Up Substrate Design

The catalyst precursor was $Co(NO_3)_2$ solution or $Fe(OH)_3$ sol solution with a concentration of 0.1 mM/L and was spin coated on the quartz substrate at a speed of 2,500 r/min. The quartz substrates containing different catalysts were placed into a 1-in tube and heated in air to 850°C for 30 min, and after the system was purged with 300 sccm argon for 5 min, a flow of hydrogen (200 sccm) and argon (300 sccm) was introduced for 20 min to reduce the catalyst precursors to form large solid Co or Fe catalysts. Then, the flow of hydrogen was changed to 300 sccm, and extra argon (10 sccm through an ethanol bubbler) was introduced to grow (n, n − 1) tubes at 850°C for 50 min or 1 h. To improve the density of the (n, n − 1) tubes, a stack-up substrate was designed as shown in Figure 1A, and in this design, the quartz substrate loaded with catalyst precursors was inverted onto Si/SiO_2 (300 nm), which is larger than the quartz substrate. During the growth of tubes, 10 sccm CO_2, 25 sccm ethanol, and 500 sccm Ar were introduced to create the near-equilibrium growth condition, and the density of the tubes was improved. This design was also applied to sapphire substrate, but the tubes were kept aligned for no reaction with CO_2. The system was cooled to room temperature with the protection of H_2 and Ar. This design was also applied to grow SWNTs with Ni, Cu, and Mo catalysts at 650°C. However, at 650°C, the C_2H_5OH/H ratio was 15/450 to grow (10, 9) tubes without CO_2, because at low temperature, the etching effect of CO_2 is much weaker.

Estimate of Carbon Nanotubes Mean Growth Rate

To compare the growth rate with different C/H ratios, *ex situ* scanning electron microscopy (SEM) was used. For different C/H ratios, we grew carbon nanotubes with different growth times and then measured the mean length of tubes by using SEM. Although the initiation and termination of tubes are not known, the time interval

could be exactly known in addition to the difference between mean lengths for different time. Therefore, the mean growth rate of carbon nanotubes could be estimated by collecting several data points before the tubes termination.

Characterizations of Carbon Nanotubes

SEM was used to characterize the morphology and density of the carbon nanotubes. AFM was used to estimate the diameter of the tubes, and the Raman spectrum with different lasers (633 and 514 nm) was adopted to distinguish the chirality of the carbon nanotubes and combined with Kataura plot after the samples were transferred on the Si/SiO_2 (300 nm) substrate. The reflection optical spectrum was done after the tubes were transferred onto the Si/SiO_2 (90 nm) substrate one by one.

Computational Models and Details

All the density-functional-theory-based calculations were performed within the framework of the Vienna Ab *initio* Simulation Package (VASP), and the exchange-correlation was parameterized with a Perdew-Burke-Ernzerhof (PBE) based on the generalized gradient approximation (GGA). The ion core-valence electron interaction was depicted by the projected-augmented wave (PAW) potential with the cutoff energy set as 400 eV. For more accuracy, all the structures were relaxed by switching on the spin polarization via the Grimme DFT-D2 method. Throughout the optimizations, the conjugated gradient algorithm was adopted, and the force convergence criterion was chosen to be 0.01 eV/Å. We calculated the formation energy of tubes on the metal surface to compare the thermodynamic stability of tubes. Given that the SWNT grown on the Co (1 1 1) surface was captured by the TEM measurement, we took the Co (1 1 1) surface as an example to study the thermodynamic stability of the tubes and the kinetic-chirality mutation from a theoretical perspective. In order to compare the formation energies of armchair tubes on the Co (1 1 1) surface, we considered a series of tubes, including (7, 7), (8, 8), (9, 9), (10, 10), and (11, 11). The definition of the formation energy of a tube is the same as that shown in previous works. For each chirality, we relaxed several stable initial configurations in order to get the global minimum. In order to void the interference of the neighboring images, we utilized a periodic supercell with volume set as 21.15 × 19.53 × 25.00 $Å^3$. Because of such a large supercell, only the Γ point in the first Brillouin region was used. In order to compare the formation energies of tubes with similar diameter on the Co (1 1 1) surface, we considered a group of tubes, including (15, 0), (15, 1), (14, 2), (14, 3), (13, 4), (13, 5), (12, 6), (11, 7), (10, 8), (10, 9), (9, 8), and (9, 9). The supercell was the same as that mentioned above. In order to calculate the energy barrier of the (9, 9) tube roughly, we assumed that the nucleation barrier occurs when the first new hexagon is formed. The formula for calculating the formation energy is referred to in previous works. The free-energy barrier of (9, 9) converted to near-armchair tubes, including (9, 8), (10, 9), and (10, 8), by inserting a 5|7 pair consisting of two parts. One is the 5|7 pair formation energy within the tube wall, and the other is the interfacial formation energy of the corresponding tubes on the Co (1 1 1) surface. The calculation method for the second part can be referred to in previous works. For the first part, a segment of (9, 9) tube with both sides passivated by hydrogen atoms was designed. At the 0^{th} step, a perfect (9, 9) with no 5|7 pair was introduced, and the total energy was labeled as E(0). By turning a C–C bond in the (9, 9) tube wall, a Stone-Wales defect can be formed with two adjacent 5|7 pairs. By continuing to rotate certain C–C bonds in the 5|7 pair, the two 5|7 pairs can depart from each other. A different 5|7 pair configuration can be formed by rotating different C–C bonds. As a result, the chirality of the segment between the two 5|7 pairs will be changed to (9, 8), (10, 9), and (10, 8).

The total energy of the system after the n^{th} rotation of the C–C bond can be labeled as E(n). Therefore, the formation energy of one 5|7 pair after the n^{th} rotation of the C–C bond can be written as follows:

$$Ef(n) = (E(n) - E(0))/2 \quad \text{(Equation 1)}$$

If the 5|7 are separated from each other by a long distance, the formation energy of the 5|7 pair will be nearly linear to the number of rotation steps of the C–C bonds. Therefore, the real 5|7 pair formation energy within the tube wall can be obtained by extrapolating the formation energy plot of the 5|7 pair when the number of rotation steps of certain C–C bonds is zero. In order to avoid the edge effect, the length of the (9, 9) is long enough.

Diffusive Model of Airflow in the Stack-Up Substrate

In our study, there was a narrow gap between the quartz substrate and Si/SiO_2 (300 nm) substrate. This gap has a height of $h \sim 20$ μm, which is more than 10^3 times less than the diameter of the furnace tube ($D \sim 2.54$ cm) used in our CVD experiments. According to the theory of fluid dynamics, the viscous flow between the gap (v) will be $(D/h)^2 > 10^6$ times slower than the flow through the furnace tube (V) or $v/V < 10^{-6}$.

In our experimental design, V is ~ 1.77 cm/s and therefore $v < 1.77 \times 10^{-8}$ m/s. This indicates that time required for the airflow to go from one side of the gap to another side (length ~ 5 mm) is $\sim 2.8 \times 10^5$ s or ~ 780 h by viscous dynamics. Then, considering the effect of molecule diffusion, the free path of the gaseous molecules under experimental condition is

$$\lambda = \frac{kT}{\sqrt{2}\pi d^2 P} = 0.17 \ \mu m, \quad \text{(Equation 2)}$$

where k is the Boltzmann constant, T = 1,123, K is the experimental temperature, d = 0.45 nm is the mean diameter of C_2H_5OH and CO_2 molecules, and $P = 10^5$ Pa is the pressure of the system. The average velocity of CO_2 and C_2H_5OH molecules in motion is

$$\langle v_m \rangle_{CO_2} = \sqrt{3kT/m} \sim 3 \times 10^2 m/s \quad \text{(Equation 3)}$$

and

$$\langle v_m \rangle_{C_2H_5OH} = \sqrt{3kT/m} \sim 3 \times 10^2 m/s, \quad \text{(Equation 4)}$$

respectively, where m is the mass of the molecule (the mass of the CO_2 and C_2H_5OH molecules is used for the estimation). So, the collision frequency between molecules can be estimated as

$$f = \frac{\langle v_m \rangle}{\lambda} = \sim 1.7 \times 10^9 \text{ Hz}. \quad \text{(Equation 5)}$$

For a molecule to diffuse out of the gap, it should travel a distance of 5 mm. Therefore, the average time for a molecule to diffuse out of the gap is

$$t = \frac{1}{f} \times \left(\frac{l}{\lambda}\right)^2 = 0.49 \text{ s}. \quad \text{(Equation 6)}$$

If the substrate is directly exposed to the gas, the time for the molecule to pass the substrate is

$$t' = \frac{l}{V} = 0.29 \text{ s}.$$

Comparing the two different times, we found that the behavior of the molecule in the gap is diffusive, and the trapping time is much longer than when exposed to the gas. This indicates that the tube growth totally depends on the molecular diffusion, which decides that the growth is slow and ensures that molecules in the stack-up substrate will react completely.

Fabrication and Measurement of Electrical Devices Based on Single Tubes

The as-grown SWNTs on quartz were transferred from quartz to a SiO_2/Si substrate with a 300-nm oxide layer according to the previously reported polymer-assisted method. Electrodes were patterned by e-beam lithography with a channel length of 2 μm. Cr (3–5 nm)/Au (50 nm) were deposited by thermal evaporation. The electrical measurement was performed by a Keithley 4200-SCS semiconductor characterization system.

SUPPLEMENTAL INFORMATION

Supplemental Information can be found with this article online at https://doi.org/10.1016/j.chempr.2019.02.012.

ACKNOWLEDGMENTS

We are grateful to R. Horn (Deakin University, Australia) for discussions. This work was supported by the Ministry of Science and Technology of China (grants 2016YFA0200101 and 2016YFA0200104), the National Natural Science Foundation of China (grants 51432002, 21790052, and 51720105003), the Beijing Municipal Science and Technology Planning Project (grant Z161100002116026), the China Postdoctoral Science Foundation (grants 8201400852 and 8201400892), the Institute for Basic Science for South Korea (grant IBS-R019-D1), and the Natural Science Foundation of Shandong Province of China (grant ZR2016EMM10).

AUTHOR CONTRIBUTIONS

J.Z. and S.Z. conceived and designed the experiments. S.Z., D.L., and Y.S. performed the growth experiments. M.H. provided the TEM data. F.D. and X.W. built the theoretical model and contributed the calculation results. F.Y. and K.L. helped perform the reflection optical spectrum. S.Z. and H.M. performed the electrical measurements. J.Z., F.D., S.Z., X.W., and Q.Z. wrote the manuscript. All authors discussed the results and commented on the manuscript.

DECLARATION OF INTERESTS

The authors declare no competing interests.

Received: November 8, 2018
Revised: December 10, 2018
Accepted: February 13, 2019
Published: March 21, 2019

REFERENCES AND NOTES

1. Franklin, A.D. (2015). Nanomaterials in transistors: from high-performance to thin-film applications. Science *349*.

2. Qiu, C., Zhang, Z., Xiao, M., Yang, Y., Zhong, D., and Peng, L.M. (2017). Scaling carbon nanotube complementary transistors to 5-nm gate lengths. Science *355*, 271–276.

3. Rutherglen, C., Jain, D., and Burke, P. (2009). Nanotube electronics for radiofrequency applications. Nat. Nanotechnol. *4*, 811–819.

4. Shulaker, M.M., Hills, G., Patil, N., Wei, H., Chen, H.Y., Wong, H.S., and Mitra, S. (2013). Carbon nanotube computer. Nature *501*, 526–530.

5. Arnold, M.S., Green, A.A., Hulvat, J.F., Stupp, S.I., and Hersam, M.C. (2006). Sorting carbon nanotubes by electronic structure using density differentiation. Nat. Nanotechnol. *1*, 60–65.

6. Chen, Y., Zhang, Y., Hu, Y., Kang, L., Zhang, S., Xie, H., Liu, D., Zhao, Q., Li, Q., and Zhang, J.

(2014). State of the art of single-walled carbon nanotube synthesis on surfaces. Adv. Mater. *26*, 5898–5922.

7. Chiang, W.H., and Sankaran, R.M. (2009). Linking catalyst composition to chirality distributions of as-grown single-walled carbon nanotubes by tuning Ni_xFe_{1-x} nanoparticles. Nat. Mater. *8*, 882–886.

8. Yang, F., Wang, X., Zhang, D., Yang, J., Luo, D., Xu, Z., Wei, J., Wang, J.Q., Xu, Z., Peng, F., et al. (2014). Chirality-specific growth of single-walled carbon nanotubes on solid alloy catalysts. Nature *510*, 522–524.

9. Sanchez-Valencia, J.R., Dienel, T., Gröning, O., Shorubalko, I., Mueller, A., Jansen, M., Amsharov, K., Ruffieux, P., and Fasel, R. (2014). Controlled synthesis of single-chirality carbon nanotubes. Nature *512*, 61–64.

10. Dresselhaus, M.S., Dresselhaus, G., and Jorio, A. (2004). Unusual properties and structure of carbon nanotubes. Annu. Rev. Mater. Res. *34*, 247–278.

11. Zhang, S., Tong, L., and Zhang, J. (2018). The road to chirality-specific growth of single-walled carbon nanotubes. Natl. Sci. Rev. *5*, 310–312.

12. Yao, Y., Li, Q., Zhang, J., Liu, R., Jiao, L., Zhu, Y.T., and Liu, Z. (2007). Temperature-mediated growth of single-walled carbon-nanotube intramolecular junctions. Nat. Mater. *6*, 283–286.

13. Zhang, S., Hu, Y., Wu, J., Liu, D., Kang, L., Zhao, Q., and Zhang, J. (2015). Selective scission of C–O and C–C bonds in ethanol using bimetal catalysts for the preferential growth of semiconducting SWNT arrays. J. Am. Chem. Soc. *137*, 1012–1015.

14. Zhang, F., Hou, P.X., Liu, C., Wang, B.W., Jiang, H., Chen, M.L., Sun, D.M., Li, J.C., Cong, H.T., Kauppinen, E.I., et al. (2016). Growth of semiconducting single-wall carbon nanotubes with a narrow band-gap distribution. Nat. Commun. *7*, 11160.

15. Kang, L., Hu, Y., Liu, L., Wu, J., Zhang, S., Zhao, Q., Ding, F., Li, Q., and Zhang, J. (2015). Growth of close-packed semiconducting single-walled carbon nanotube arrays using oxygen-deficient TiO_2 nanoparticles as catalysts. Nano Lett. *15*, 403–409.

16. Che, Y., Wang, C., Liu, J., Liu, B., Lin, X., Parker, J., Beasley, C., Wong, H.S., and Zhou, C. (2012). Selective synthesis and device applications of semiconducting single-walled carbon nanotubes using isopropyl alcohol as feedstock. ACS Nano *6*, 7454–7462.

17. Li, J., Liu, K., Liang, S., Zhou, W., Pierce, M., Wang, F., Peng, L., and Liu, J. (2014). Growth of high-density-aligned and semiconducting-enriched single-walled carbon nanotubes: decoupling the conflict between density and selectivity. ACS Nano *8*, 554–562.

18. Yao, Y., Feng, C., Zhang, J., and Liu, Z. (2009). "Cloning" of single-waled carbon nanotubes via open-end growth mechanism. Nano Lett. *9*, 1673–1677.

19. Liu, J., Wang, C., Tu, X., Liu, B., Chen, L., Zheng, M., and Zhou, C. (2012). Chirality-controlled synthesis of single-wall carbon nanotubes using vapour-phase epitaxy. Nat. Commun. *3*, 1199.

20. Wang, H., Ren, F., Liu, C., Si, R., Yu, D., Pfefferle, L.D., Haller, G.L., and Chen, Y. (2013). CoSO4/SiO2 catalyst for selective synthesis of (9, 8) single-walled carbon nanotubes: Effect of catalyst calcination. J. Catal. *300*, 91–101.

21. Zhang, S., Kang, L., Wang, X., Tong, L., Yang, L., Wang, Z., Qi, K., Deng, S., Li, Q., Bai, X., et al. (2017). Arrays of horizontal carbon nanotubes of controlled chirality grown using designed catalysts. Nature *543*, 234–238.

22. Zhao, Q., Xu, Z., Hu, Y., Ding, F., and Zhang, J. (2016). Chemical vapor deposition synthesis of near-zigzag single-walled carbon nanotubes with stable tube-catalyst interface. Sci. Adv. *2*, e1501729.

23. Reich, S., Li, L., and Robertson, J. (2006). Control the chirality of carbon nanotubes by epitaxial growth. Chem. Phys. Lett. *421*, 469–472.

24. Artyukhov, V.I., Penev, E.S., and Yakobson, B.I. (2014). Why nanotubes grow chiral. Nat. Commun. *5*, 4892.

25. Ding, F., Harutyunyan, A.R., and Yakobson, B.I. (2009). Dislocation theory of chirality-controlled nanotube growth. Proc. Natl. Acad. Sci. USA *106*, 2506–2509.

26. Yuan, Q., and Ding, F. (2015). How a zigzag carbon nanotube grows. Angew. Chem. Int. Ed. *54*, 5924–5928.

27. Yuan, Q., Xu, Z., Bi, Y., and Ding, F. (2012). Efficient defect healing in catalytic carbon nanotube growth. Phys. Rev. Lett. *108*, 245505.

28. Ding, F., Xu, Z., Yakobson, B.I., Young, R.J., Kinloch, I.A., Cui, S., Deng, L., Puech, P., and Monthioux, M. (2006). Formation mechanism of peapod-derived double-walled carbon nanotubes. Phys. Rev. B *82*, 041493.

29. Liu, Y., Wei, N., Zeng, Q., Han, J., Huang, H., Zhong, D., Wang, F., Ding, L., Xia, J., Xu, H., et al. (2016). Room temperature broadband infrared carbon nanotube photodetector with high detectivity and stability. Adv. Opt. Mater. *4*, 238–245.